Catalysis Today 284 (2017) 160–168

Contents lists available at ScienceDirect

Catalysis Today

journal homepage: www.elsevier.com/locate/cattod

Carbon sphere templates for TiO_2 hollow structures: Preparation, characterization and photocatalytic activity

Balázs Réti [a], Gabriella Ilona Kiss [a], Tamás Gyulavári [a], Kornelia Baan [b], Klara Magyari [c], Klara Hernadi [a,d,*]

[a] Department of Applied and Environmental Chemistry, Faculty of Sciences and Informatics, University of Szeged, Rerrich tér 1, H-6720 Szeged, Hungary
[b] Department of Physical Chemistry and Material Science, University of Szeged, Tisza Lajos krt. 84, H-6720 Szeged, Hungary
[c] Interdisciplinary Research Institute on Bio-Nano-Sciences, Babes-Bolyai University, M. Kogalniceanu 1, 400084 Cluj-Napoca, Romania
[d] Research Group of Environmental Chemistry, Institute of Chemistry, Faculty of Sciences and Informatics, University of Szeged, Dóm tér 7, H-6720 Szeged, Hungary

ARTICLE INFO

Article history:
Received 21 June 2016
Received in revised form 22 October 2016
Accepted 21 November 2016
Available online 28 November 2016

Keywords:
Carbon spheres
Titanium dioxide
Hollow structure
Photocatalysis
Phenol

ABSTRACT

TiO_2 hollow structures (HS) were synthesized by carbon sphere template removal method. Nanometer sized carbon spheres (CS) were prepared by mild hydrothermal treatment of ordinary table sugar (sucrose). The size of these spheres can be controlled by the parameters of the hydrothermal treatment (e.g. time and pH). The obtained CSs were characterized by scanning electron microscopy (SEM), Raman spectroscopy, infrared spectroscopy (IR), X-ray diffraction (XRD) and thermogravimetry (TG). CSs were successfully coated with TiO_2 via sol–gel method. The phase composition of the TiO_2 hollow spheres were controlled by the annealing temperature during crystallization and CSs template removal. TiO_2 hollow structures (HSs) were characterized by SEM, XRD, Raman spectroscopy, TG and energy-dispersive X-ray spectroscopy (EDX). Photocatalytic performance of the TiO_2 HSs was evaluated by phenol degradation in a batch-type foam reactor under low powered UV-A irradiation. The degradation reaction was followed by high-performance liquid chromatography (HPLC) and total organic carbon (TOC) measurement techniques. Photocatalytic activity test results pointed out that increased rutile content up to a certain extent (resulting mixed phase anatase-rutile TiO_2) effects advantageously the photocatalytic performance of TiO_2 HSs and the unique morphology proved to enhance the photocatalytic activity (six times) as well as TOC removal efficiency (twelve times) compared to the sample which was prepared by the same method without the CSs.

1. Introduction

Since the industrial revolution the water pollution gradually became more and more significant, and nowadays it is a burning environmental issue [1,2]. Among the many hazardous water pollutants [3,4], phenol is one of the most studied because it can be originated from both anthropogenic and natural sources [5–7]. The purification of this essential media is imperative. Fortunately, there are already many effective technological and technical solutions to achieve the elimination of various water contaminants. However, there are chemicals which are not removable from water by conventional methods due to their stability and/or toxicity towards microorganisms (e.g. pesticides, antibiotics, pharmaceutical metabolites, etc.). Advanced oxidation processes (AOPs) are effective methods for the neutralization of these persistent contaminants [8]. Heterogeneous photocatalysis is a promising branch of AOP technologies.

Titanium dioxide (TiO_2) is an n-type semiconductor transition metal oxide possessing many advantageous properties to be considered one of the most promising photocatalyst materials [9,10]. It is cheap, photostable, non-toxic and biocompatible. Heterogeneous photocatalysis is a very complex photoinduced process on the surface of semiconductor particles [11–14]. During the photoexcitation of a semiconductor particle with energy equal or greater than its band gap (E_g) an electron is excited to the conduction band (CB) from the valence band (VB) leaving a vacancy (hole; h^+) behind. TiO_2 polymorphs possess inherently different band gap energies ($E_g \sim 3.2$ eV = 388 nm; $E_g \sim 3.0$ eV = 413 nm for anatase and rutile, respectively) [15]. The photogenerated charge carriers (e^- and h^+)

* Corresponding author at: Department of Applied and Environmental Chemistry, Faculty of Sciences and Informatics, University of Szeged, Rerrich tér 1, Szeged H-6720, Hungary.
E-mail address: hernadi@chem.u-szeged.hu (K. Hernadi).

http://dx.doi.org/10.1016/j.cattod.2016.11.038
0920-5861/

are capable to migrate to the surface of the particle or being trapped at various sites [13]. If the charge carriers are able to reach the surface they may take part in redox reactions with appropriate donor and acceptor species. In aqueous media, important donor and acceptor molecules are OH^- (H_2O) and dissolved O_2, respectively, and they form highly reactive and oxidative $OH^\bullet$ and $O_2^{\bullet-}$ radicals [16]. The overall photocatalytic activity of a material is dependent of many factors [17]. In most cases, crystal phase composition is determinative regarding the photocatalytic performance. However, mixed phase (particularly anatase-rutile) TiO_2 photocatalysts may possess elevated activities most presumably due to their interfacial interactions [18–24].

There is a tremendous effort in the investigation of carbon (nano)materials since the discovery of fullerenes [25]. Researchers prepared carbon materials with various sizes and shapes (e.g. fibers, onions, horns, (nano)tubes, etc.) [26]. Carbon spheres (CS) are recently regained scientific interest due to their promising application in battery cathodes [27], fuel cells [28] and catalyst supports [29,30]. CSs can be prepared by numerous synthesis techniques: arc-discharge, CVD, hydrothermal method etc. [31]. A convenient route to produce micro- or nanosized CSs is the hydrothermal dehydration and carbonization of different carbohydrates (most commonly glucose) [32,33].

Titanium dioxide hollow spheres can be prepared by using the abovementioned CSs as removable templates. Thus, the diameter of the TiO_2 hollow structures is finely tunable. These objects are interesting not just because there low apparent density [34] but their unique optical properties [35–37]. These attributes can be exploited in either photocatalytic applications or in DSSCs [38]. As mentioned, the most commonly used route to prepare TiO_2 (and other metal oxide) hollow spheres is template removal method [39]. Lv et al. studied the efficiency of surface fluorinated TiO_2 HS prepared via hydrolysis–precipitate method (using sulfonated polystyrene beads as templates) in brilliant red X3B photocatalytic degradation reaction [40]. Ao et al. prepared TiO_2 HSs by precipataion of TiO_2 onto the surface of hydrothermally prepared CSs and demonstrated enhanced photocatalytic activity in photocatalytic decomposition of methylene blue [41].

Herein, we describe the preparation of carbon sphere templates from ordinary table sugar via facile hydrothermal method and their use as templates for TiO_2 hollow structure synthesis. We intended to investigate the effect of various synthesis parameters (time, pH) on the yield and size of the CSs. The CS sample with appropriate size distribution was selected as removable template for the preparation of TiO_2 hollow structures. We have studied the crystal phase composition of the hollow spheres formed during heat treatment at different temperatures and the effect of this parameter on their photocatalytic activity in phenol decomposition reaction.

2. Experimental

2.1. Materials

All chemicals were used as received without further purification. During the experiments, Milli-Q water (Millipore, 18.2 MΩ cm) and absolute ethanol was used (VWR Prolabo). *Carbon sphere synthesis*: Ordinary table sugar (sucrose, Magyar Cukor Zrt., Koronás™) was used as carbon source. The desired pH was adjusted with hydrochloric acid (37 wt%, a.r., Molar) or with sodium hydroxide (50 wt%, a.r., Molar). *TiO_2 hollow structure synthesis*: The titanium precursor was titanium(VI) butoxide (Fluka, ≥97% purum, $[Ti(O\text{-}CH_2CH_2CH_2CH_3)_4]$). *Photocatalytic test reactions*: The model pollutant was phenol (VWR, extra pure) and during the experiments oxygen gas (Messer, 2.5) was used. Methanol (VWR HiperSolv Chromanorm) was used during the eluent preparation for the HPLC analysis.

2.2. Sample preparation

First, CSs were synthesized via hydrothermal treatment. All hydrothermal experiments were carried out in a preheated drying oven at 180 °C using a Teflon-lined stainless steel autoclave with total volume of 275 cm^3. During each CS preparations, 80 cm^3 of 50 g/dm^3 sucrose solution was treated (V_{fill}/V_{tot} = 29%). The effect of hydrothermal treatment time (3, 6, 12, 18 h) was studied on the resulted product. To investigate the effect of pH, the sucrose solution was adjusted by HCl or NaOH solutions to achieve the desired values (3, 7, 12; for the sake of notation, the unmodified sucrose solution will be considered as pH 7 since sucrose does not inherently change the pH when dissolved in water, thus the pH of this solution is ~7). After the hydrothermal treatment, the autoclave was left to cool to room temperature naturally, then the brownish-black product was collected. The samples were centrifuged (4000 rpm, 20 min) and redispersed in water three times. Then, they were filtered with a membrane filter apparatus (Millipore, Durapore PVDF membrane, 47 mm, 0.1 μm) and washed with hot water, than with three aliquot 5, 15, 45 V/V% ethanol/water mixtures to remove residual organic contaminants. The solid product was dried in air at 70 °C for 18 h. Sample labeling for the CSs will be the following: CS-t-pH, where 't' is the time of hydrothermal treatment, 'pH' is the pH of the starting sucrose solution.

The CS sample with the preferred properties was used as a template for the synthesis of TiO_2 hollow structures. 2 g of the CSs was suspended in 130 cm^3 ethanol via ultrasonication and 0.64 cm^3 water was added to the suspension (named as mixture "A"). 4 cm^3 titanium(IV) butoxide was added to 70 cm^3 absolute ethanol under vigorous stirring (named as mixture "B"). Mixture "B" was added drop by drop (~2 cm^3/min) to mixture "A" under vigorous stirring. The molar ratio was $n(Ti):n(H_2O) = 1:3$. After the full addition of the two mixtures, it was left to be stirred for 1 h and then it was filtered and washed with 10 cm^3 ethanol three times. The product was dried in air at 70 °C for 18 h. The above described process was repeated three times and the portions were united. The whole coating process was repeated under the same conditions expect that for starting material was the previously coated carbon spheres (instead of pristine CSs) and all precursor, ethanol and water quantities were tripled. Aliquot amount of samples were annealed in a static furnace in air with a heating rate of 5 °C/min for 4 h at 400, 500, 600, 700 °C to remove the CS core and simultaneously convert the amorphous titania phase to crystalline TiO_2. TiO_2 reference sample was prepared via exactly the same method as TiO_2 HSs were, except that during the synthesis procedure CSs were not added. Reference sample was calcinated with heating rate of 5 °C/min for 4 h at 500 °C in air. (Characterization of the reference TiO_2 can be found in Supplementary material.)

2.3. Characterization techniques

The structure and morphology of the prepared samples was investigated with scanning electron microscopy (Hitachi S-4700 Type II FE-SEM). Crystal structure and phase composition was measured with X-ray diffractometry (Rigaku MiniFlex II Diffractometer) using Cu Kα radiation. Thermogravimetric analysis (Netzsch STA 409 PC connected to a Pfeiffer QMS 200 mass spectrometer system) was performed in oxygen flow (40 cm^3/min) with 5 °C/min heating rate using ~100 mg sample. Raman spectrum was taken (Thermo Scientific DXR Raman Microscope) utilizing 532 nm laser irradiation. FT-IR spectrum was taken using a Biorad FTS-60A FT-IR device using an ATR module on an air-dry sample. The concentration of phenol was measured with a HPLC technique (Merch Hitachi sys-

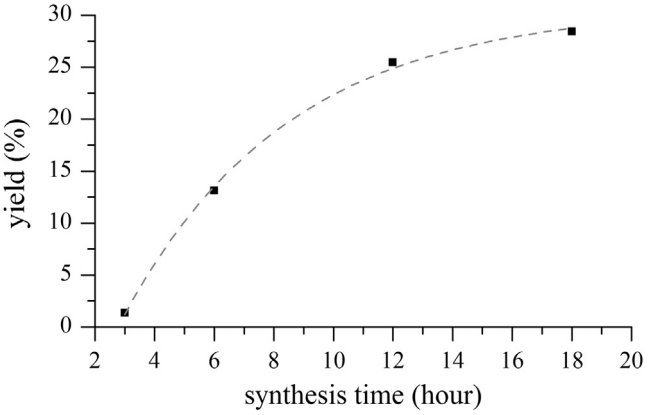

Fig. 1. The effect of synthesis time on the yield of the carbon spheres.

tem). LiChrospher RP-18e column and V(methanol):V(H_2O) = 1:1 eluent was used during the HPLC analysis. Total organic carbon content of phenol solution was determined before and after (samples were centrifuged first) the photocatalytic test reactions (Analytik Jena Multi N/C 3100).

2.4. Evaluation of photocatalytic efficiencies

Photocatalytic degradation of the phenol model pollutant was carried out in a cylindrical shape batch-type suspension foam reactor equipped with thermostating jacket made from glass. The diameter of the inner tube was 45 mm (V = 250 cm^3). To provide sufficient mixing and dissolved oxygen level, oxygen gas was bubbled though a fritted glass to the solution with flow rate of 430–450 cm^3/min. The UV-A lamp (Sylvania Blacklight F6W/T5/BL350) was immersed in the center in a quartz tube (25 mm in diameter). All photocatalytic experiments were performed at 25 ± 0.5 °C. The initial phenol concentration and the photocatalyst load was 1×10^{-4} mol/dm^3 and 0.5 g/L, respectively. The photocatalyst sample was added to the 200 cm^3 1×10^{-4} mol/dm^3 phenol solution and sonicated for 5 min then transferred to the photoreactor. The photocatalyst suspension was left to be stirred in dark for 30 min to reach adsorption/desorption equilibrium. At that point, the UV lamp was switched on and samples were taken in regular time intervals. Total irradiation time was 90 min. Each photocatalytic experiments were done in duplicate to check reproducibility.

After the experiment, the acquired samples were centrifuged at 16000 RCF. Each sample was filtered by a syringe filter (Whatman, Anotop 25+, 0.02 μm) to remove even the fines particles prior the HPLC analysis (0.9 cm^3/min flow rate, UV–vis detection at 210 nm). TOC content was determined to evaluate the overall mineralization potential of the photocatalysts.

3. Results and discussion

3.1. Carbon spheres

3.1.1. The effect of synthesis time

First, as an important aspect of any synthetic procedure, the effect of the duration of hydrothermal treatment was studied on the yield and the size distribution of the CSs. After the preparation of CSs, the yield (defined as $m_{CS}/m_{sucrose}$) was calculated and its dependence on the synthesis time is shown in Fig. 1. By the end of the three hour reaction the yield was very low (1.4%), which can be explained by the low nucleation rate of the CS seeds. Increased reaction time leads to increased yield, but after twelve hours the change in yield is lessening and most probably leading to saturation due to the consumption of the sucrose (according to our data the estimated maximum yield is around 30%). Based on these finding, sufficient yields are achievable by applying at least 12 h reaction time. The morphology and size (diameter) of the CSs were investigated by SEM technique (Fig. 2). After just three hours of reaction time (CS-3-7), well-defined sphere structures were observed. The particle size distribution was rather narrow; most of the spheres had a diameter around 350 nm. Six hours of hydrothermal treatment resulted similar product (CS-6-7) compared to the sample CS-3-7. The rather narrow size distribution is shifted towards bigger particle sizes; the average particle size was around 590 nm. The size distribution of the CS-12-7 sample was wider compared to the previously mentioned one; as well as the average size of the spheres was increased to ~660 nm. In this sample joint spheres were formed but they could be observed in a relatively low amount. On the SEM picture of CS-18-7, CSs with greater size were also detectable, and joint structures were more prominent. The average size of the spheres is increased to ~700 nm and wider size distribution could be observed. Overall, at shorter synthesis times the nucleation of CSs was more significant, and later on the nucleation slowed down and the growth of CS became the dominant process. Combining the experiences with the ones regarding the yields, further experiments were done with 12 h of synthesis time.

3.1.2. The effect of pH

After finding the most convenient but satisfactory synthesis time, the effect of pH was investigated on the morphology of the CSs. The pH values of the sucrose solutions were set to 3 and 12 before the hydrothermal treatment (sample with pH 7, CS-12-7, has already been demonstrated in the previous section). The yield of these synthesizes were 23%, 26% and 28% for the CS-12-3, CS-12-7, CS-12-12, respectively. Only a slight increase was noticeable with increasing pH. Fig. 3 shows conspicuously the difference between the CS-12-3 synthesized under acidic, and the CS-12-12 under basic conditions. CS-12-3 sample prepared in acidic media showed quite wide particle size distribution and have an average particle size around 810 nm. Larger, joint particles are also present in the sample. CS-12-7 sample own similar particle size distribution to CS-12-3, however, the average particle size was decreased to around 660 nm. CS-12-12 sample showed narrower size distribution compared to the previously discussed samples. The average particle size was around 400 nm and the presence of joint particles was not prominent. According to these results it can be concluded that the pH of the sucrose solution has significant impact on the size of the prepared CSs. A plausible explanation of the phenomenon can be the following: Sucrose first undergoes dehydration reaction resulting HMF (5-(hydroxymethyl)-2-furaldehyde) which then take part in polymerization and aldol condensation reactions [32,33,42]. It is reported that aldol reaction of cyclic and aromatic ketones/aldehydes are more favorable under alkaline conditions [43]. Thus, this may lead to faster accumulation of polymerized species which eventually results rapid nucleation. Subsequently, particle growth is more decisive in the later period of the hydrothermal process resulting increased number of smaller particles. In acidic media, the nucleation is somewhat elongated, followed by particle growth resulting larger particles and wide particle size distribution. Since CS-12-12 sample showed good yield and quite uniform CSs it has been studied further and used as template for the preparation of TiO_2 hollow structures.

3.1.3. Characterization of CSs

CS-12-12 sample was studied with various techniques (Fig. 4). XRD was used to investigate the possible crystallinity of the CSs (Fig. 4, A). Only one broad diffraction at ~22° dominates the diffractogram which belongs to amorphous carbon [44]. Reflection at

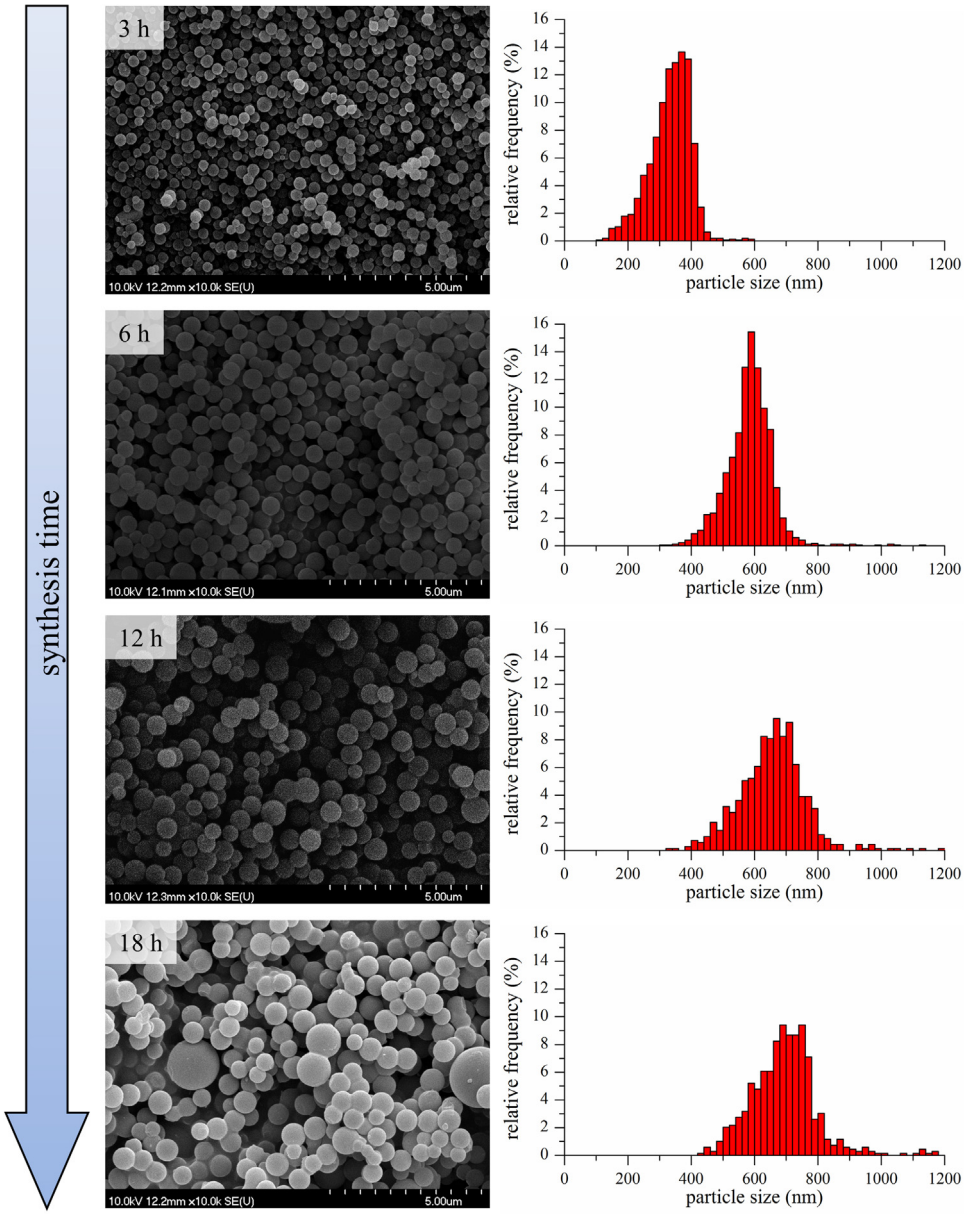

Fig. 2. Morphology of carbon spheres prepared via hydrothermal treatment at different synthesis times (indicated in the upper left corner of the SEM pictures). Particle size distributions of CSs are shown on the histograms right to the corresponding SEM pictures. Please note that the SEM micrographs and the histograms are directly comparable due to their same scale and formatting.

~26.5° was not detected which would indicate well-structured graphitic segments. No crystalline impurities were detected.

Raman spectroscopy was used to analyze the CSs (Fig. 4B). In the Raman spectra, typical Raman features of carbon materials were present, namely the D (~1350 cm^{-1}) and G (~1580 cm^{-1}) bands. While the D band can be attributed to the presence of sp^3 hybridized carbon atoms, the G band is an indicator of conjugated sp^2 carbon atoms. In highly graphitic carbon materials 2D band (~2700 cm^{-1}) is also present, however it is missing from the Raman spectra of the CSs. Both D and G bands are broad, meaning a rather amorphous structure. The high intensity G band compared to the D band indicates that most of the material consists of conjugated carbon framework.

FT-IR technique was used to further investigate the chemical characteristics of the CSs (Fig. 4C). The spectrum is feature-rich and quite complex. Broad band appear in the 1800–3800 cm^{-1} which indicates the stretching vibrations of structural OH groups and physisorbed water. Low intensity bands at around 2922 and 2970 cm^{-1} can be assigned to C—H stretching vibrations. The very intense band situated at 1701 cm^{-1} belongs the C=O stretching vibrations. Another intense band at 1611 cm^{-1} is most probably the sign of the C=C vibration in aromatic ring; however, some oxygen containing groups (e.g. cyclic ethers) could appear in the same region [45]. Intense and broad band is present between 1100 and 1400 cm^{-1} which indicates C—O vibration in highly conjugated, aromatic or in various other chemical environments [46].

The thermal behavior of CSs was also investigated (Fig. 4D). Heating the CSs in oxygen atmospheres two intense weight loss can be seen. The first is between 220 and 250 °C, the second is 410–440 °C and the two regions are linked with a moderate mass-reducing period. The former is most probably due to the decomposition of various oxygen containing functional groups while the latter is due to the combustion of the carbon itself [47,48].

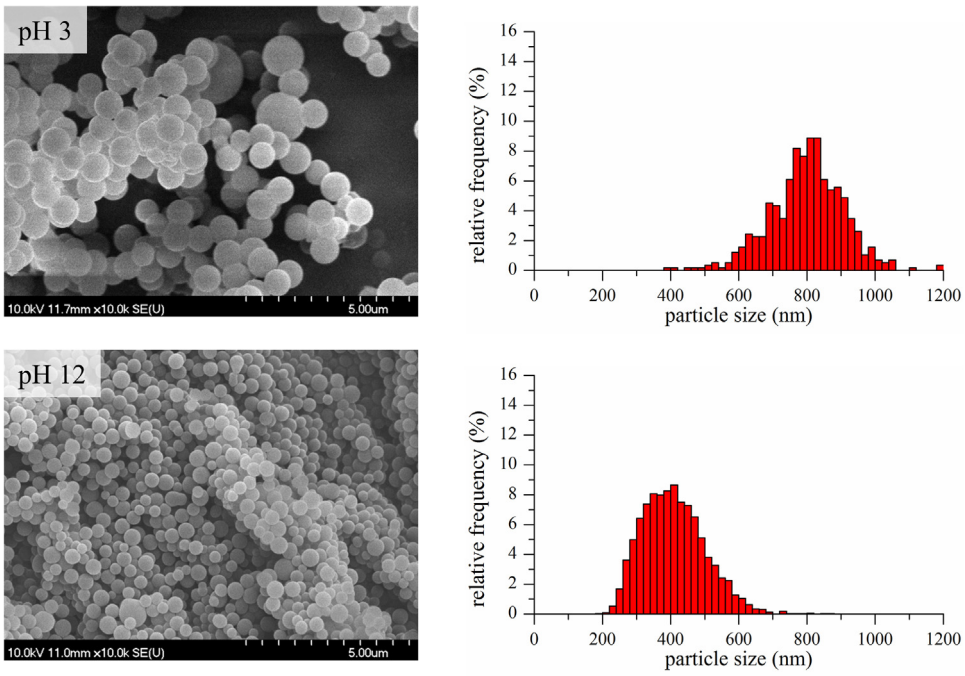

Fig. 3. The effect of pH on the morphology of the prepared carbon spheres. Please note that the SEM micrographs and the histograms are directly comparable due to their same scale and formatting.

The low decomposition and combustion temperature is convenient in case of the removal of these template materials.

According to our results, CSs were consist of amorphous carbon with no graphitic domains. However, Raman and FT-IR results indicated significant conjugated/aromatic segments as well as various oxygen containing functional groups.

3.2. Titanium dioxide hollow structures

CS-12-12 carbon sphere sample were coated with TiO_2 layer via sol-gel method. This material was then calcinated in air to remove the CS template and to convert the amorphous titania into crystalline titanium dioxide. Elaboration of TiO_2 HSs from as-prepared, non-heat-treated (nht) CS-titania was studied by TG-MS technique (Fig. 5). The TG-DTG showed similar features to the TG-DTG of uncoated CSs (Fig. 4D). The first major, well defined weight losing period was at around ~220–250 °C while the second was a more elongated, broad region which was started right after the first one and was between ~250–480 °C. The elongated combustion of CS templates compared to uncoated CSs can be attributed to the presence of TiO_2 shell. Above ~480 °C, no weight-change can be detected. The remaining 27.4% mass is contributed to the incombustible crystalline TiO_2. The weight loss was approximately 73% independently from the calcination temperature in case of all TiO_2 HSs. Consequently, if at 700 °C CSs and all combustible compounds are burned away; and there is no variation in the weight loss between the calcination temperatures then no organic residue from the precursor/solvent or CSs is left in TiO_2 HS, not even at the lowest temperature. This was further confirmed by the MS results (Fig. 5, right panel). CO and CO_2 were identified as main gaseous products. The temperature range of the evolution of the two gases is identical to the main mass reduction regions mentioned in TG-DTG results. Thus, considering the weight losing rate and the MS results it can be deduced that even at 400 °C 4 h of calcination time is enough to completely eliminate all carbon, not to mention higher temperatures.

Fig. 6 shows the morphology of the TiO_2 hollow structures annealed at different temperatures. Round forms, whole and damaged structures can be seen in the pictures. Smaller, fragmented shell particles are scattered between larger hollow spheres. Shell thickness is between 20 and 40 nm regardless of the annealing temperature. This thickness is thick enough to preserve the shape of the template and thin enough to be permeable for the photons to exploit the special shape of the object.

Crystallinity of the TiO_2 samples was investigated by XRD technique (Fig. 7). Diffraction intensities of the individual diffractograms were normalized to the intensity of anatase (101) reflection. All samples show characteristic, rather sharp reflections marked with the appropriate Miller indices. In case of the samples annealed at 400 °C and 500 °C only anatase phase TiO_2 is present. As expected, at higher temperatures rutile phase was formed. Rutile content of samples calcinated at 600 °C and 700 °C were calculated according to the well-known equation determined by Spurr et al. [49] and they contained 37 w/w% and 65 w/w% rutile, respectively. Full width at half maximum (FWHM) of anatase (101) reflection is decreasing proportionally with the increasing heat treatment temperature from 0.47° to 0.26°, from 400 °C to 700 °C respectively. It can be deduced that a more ordered, well-crystallized structure provides less recombination centers for the photogenerated e^-/h^+ pairs. At 600 °C, rutile phase TiO_2 appears. FWHM of rutile (110) reflection was decreased from 0.28° to 0.22°, from 600 °C to 700 °C respectively. Based on the X-ray diffractograms, the crystallite sizes were determined using the Scherrer equation (see Supplementary material Table S01). As anticipated, the crystallite sizes increased gradually with increasing annealing temperature.

Specific surface area of TiO_2 HS samples was determined by BET method (see Supplementary material Table S01). Also, detailed measurement was executed on a representative sample of TiO_2 HS (annealed at 600 °C) in order to investigate not just the specific surface area but also the pore structure (Fig. 8). The specific surface area and the total pore volume were found to be 26 m^2/g and 0.14 cm^3/g, respectively. The obtained specific surface area values of TiO_2 HSs are rather small compared to porous metal oxide

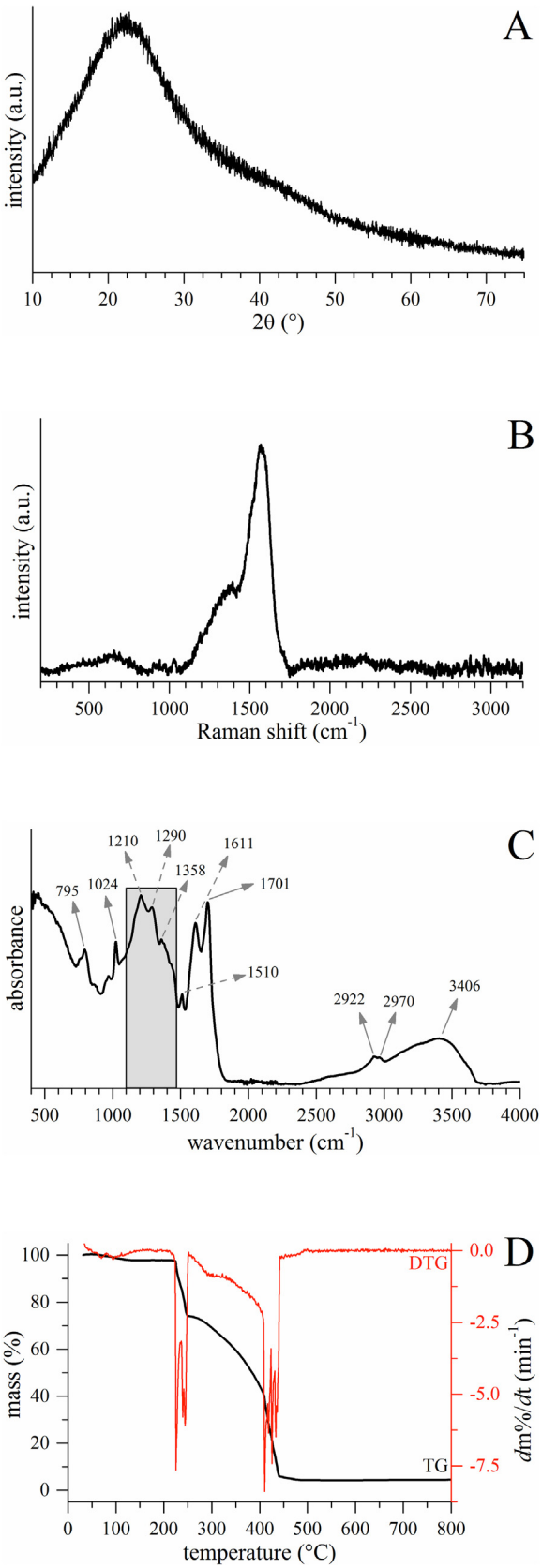

Fig. 4. X-ray diffraction pattern, Raman and FT-IR spectra and TG curve of CS-12-12 are shown from top to bottom, labeled A–D, respectively.

materials [50]. The specific surface area can be roughly approximated to gain information on the magnitude of the specific surface area of spherical hollow objects. Assuming non-porous, perfectly spherical shell of anatase which can be elaborated on the surface of D = 400 nm CSs with thickness of 30 nm, the specific surface area is calculated 17 m^2/g which is in reasonable agreement with the obtained specific surface area values of TiO_2 HSs (see Table S01). The N_2 adsorption measurement revealed the presence of meso- and macropores; however, the order of magnitude of these pore volumes is rather small (10^{-4} cm^3 nm^{-1} g^{-1}). Thus, they have only small contribution to specific surface area. There is a decreasing trend in the specific surface area of the TiO_2 HSs with increasing annealing temperature. This is due to the consolidation, densification and sintering of the TiO_2 particles/crystallites and TiO_2 HSs as well.

Briefly, crystalline TiO_2 hollow structures were prepared via complete removal of CS templates at different temperatures. Independently from the annealing temperature, the hollow spheroid shape was preserved; however, in some extent the spheres were fragmented. The TiO_2 HSs does not show well-defined pore structure and it can be considered as rather solid/dense shell of TiO_2 with a hollow inside.

3.3. Photocatalytic activity

Photocatalytic performance of the prepared TiO_2 HSs was investigated with the photocatalytic decomposition reaction of phenol under low powered UV-A irradiation. The photocatalytic activity was represented by the apparent rate constant (k_{app}). This was calculated from the first 40 min irradiation period by linear fitting of the $-\ln(c/c_0)$ *vs* t relation assuming pseudo first order reaction kinetic. Phenol photocatalytic degradation curves as well the photocatalytic activities are summarized in Fig. 9. All prepared TiO_2 HS samples have shown considerable photocatalytic activity in phenol degradation reaction. Since no carbon contamination originated from the used titanium precursor, solvents and CSs were detected the effect of such impurity on the photocatalytic activity is improbable. N_2 adsorption measurements showed the specific surface area of the TiO_2 HSs is decreasing with increasing calcination temperature which indicates that TiO_2 HS 700 °C has high photocatalytic activity despite of its rather low specific surface area. Photocatalytic activity was increased parallel to the calcination temperature which can be explained by the crystallization of the samples. With the appearance of rutile phase the photocatalytic activity has increased further to a certain limit. Light absorption properties of the TiO_2 HS samples were investigated by diffused reflectance spectroscopy (see Supplementary material Fig. S08). In case of titanium dioxide hollow structures, the results indicated increased light harvesting feature in the most of the UV region compared to the dense reference sample. This higher light absorption (appear as lower reflectance in Fig. S08) can contribute to the elevated photocatalytic efficiency of TiO_2 HS contrary to dense TiO_2 reference sample.

It is well-known that the coexistence of anatase and rutile phase can enhance the photocatalytic activity. The increased photocatalytic activity of mixed anatase/rutile phase TiO_2 is due to the difference in the band position of anatase and rutile as well as to the solid-solid interface can greatly influence the photogenerated charge carrier separation. This interface is responsible for fast charge carrier diffusion to the surface of the particle thus influencing the charge transfer and recombination processes [51,52]. Also, it is believed that rutile phase is able to accept electrons from anatase phase, thus acting as an “electron sink” since this process is thermodynamically favorable to their band positions [53].

Total organic carbon removal capability was also studied. The change of TOC removal efficiency and the photocatalytic activity

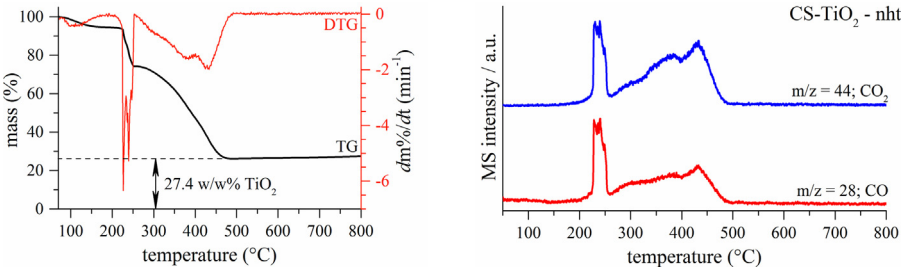

Fig. 5. TG-DTG curve (left) and MS results (right) of non-heat-treated titania coated CSs.

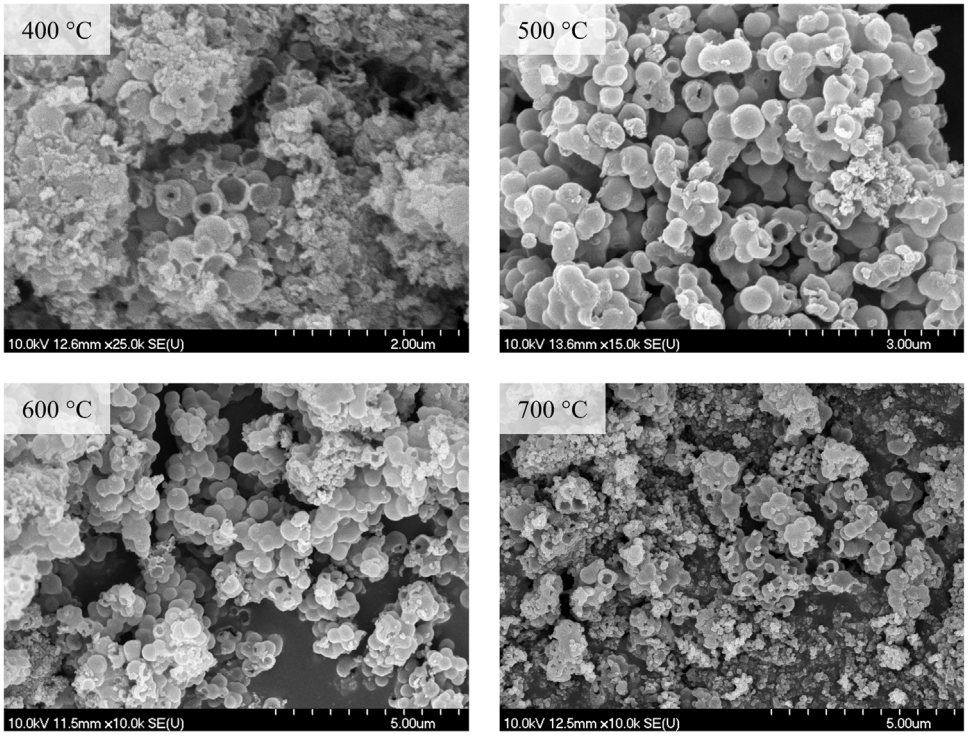

Fig. 6. Morphology of the TiO_2 hollow structures annealed at different temperatures.

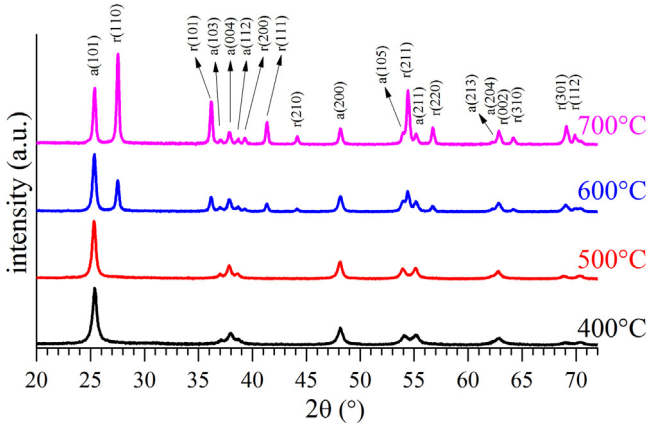

Fig. 7. X-ray diffraction pattern of TiO_2 hollow structures annealed at different temperatures.

was in good agreement. High percentage of TOC removal indicates not just efficient phenol degradation but also potent mineralization properties. A small drop of TOC removal efficiency was noticed in case of the TiO_2 HS annealed at 700 °C which can be explained by the different photodegradation pathway of mineralization of phenol on anatase and rutile phase TiO_2 [54]. Thus, for applications where efficient mineralization of organic contaminants is desired mixed phase TiO_2 can be used advantageously.

As a reference, a TiO_2 sample was prepared with the same method as the TiO_2 HSs but without CS template. The photocatalytic activity of this sample could be compared to the TiO_2 HS calcinated at the same temperature (500 °C). As a result, TiO_2 HS showed 6 times higher photocatalytic activity and 12 times higher TOC removal efficiency during 90 min UV-A irradiation compared to its counterpart prepared without CS template. Thus, addition of CS template to an existing TiO_2 preparation method makes huge difference in photocatalytic activity that is definitely worth exploiting as the results indicated.

4. Conclusion

In this work, we report the successful preparation of titanium dioxide hollow structures by removal of carbon sphere templates synthetized via hydrothermal treatment of sucrose solution using ordinary table sugar. Firstly, hydrothermal synthesis parameters of CS preparation were investigated emphasizing on the reaction time and the pH of the sucrose solution. Both factors have determinative effect on the size distribution of the CS product. Increasing reaction time resulted increased yield and particle size as well. The

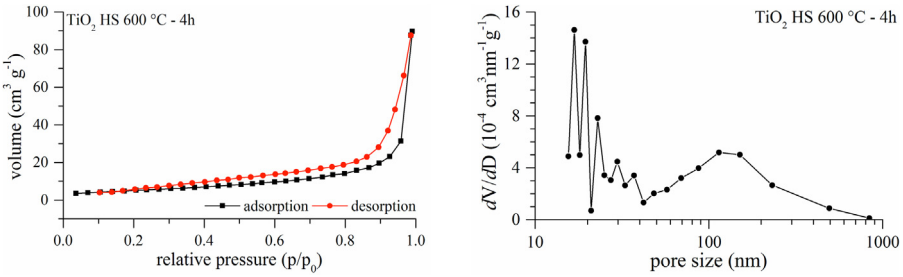

Fig. 8. N_2 adsorption measurement (left) and pore size distribution (right) of representative TiO_2 HS sample (calcinated at 600 °C).

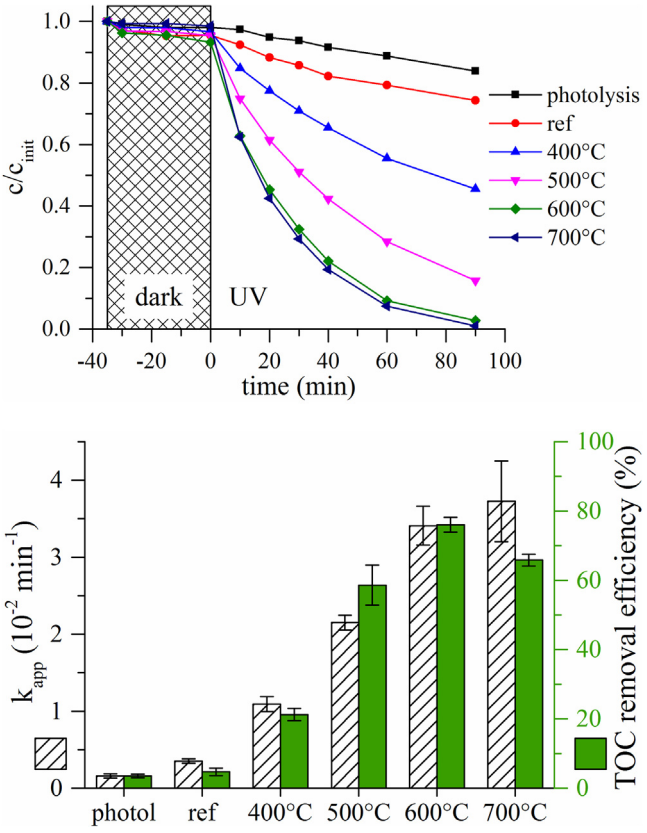

Fig. 9. Phenol photocatalytic degradation curves of the different TiO_2 hollow structure samples (top). Photocatalytic activity [striate column] and total organic carbon content removal efficiency [dense column] of the TiO_2 hollow structure samples (bottom).

study on the effect of initial pH of the sucrose solution revealed that under acidic conditions larger CSs are formed; however, in alkaline media smaller, more homogeneous particle size was achieved and the average particle size was around 400 nm with acceptable yield. Characterizations of the CSs revealed that these spheres consist of amorphous carbon. However, they contain significant amount of conjugated/aromatic segments and various oxygen containing function groups which is advantageous for the preparation of TiO_2 shells on their surface. CSs were coated with TiO_2 via sol-gel method and calcinated at different temperatures to remove the inner carbon sphere core and to convert the amorphous titania layer into crystalline TiO_2. TiO_2 hollow structures were obtained and their morphology was investigated. After annealing, the spherical characteristic was preserved and TiO_2 shells with 20–40 nm thickness were formed. As expected, some imperfect and fragmented shell structures were also present. Photocatalytic activity of the TiO_2 HS was studied by phenol degradation reaction under low-powered UV-A irradiation. All TiO_2 HS samples showed significant photocatalytic activity as well as good mineralization efficiency measured by TOC technique. TiO_2 HSs containing rutile phase (along with anatase) showed even higher photocatalytic activity compared to only anatase containing ones most probably due to synergic effect between the two polymorphs. TiO_2 hollow structure photocatalyst proved to have six times higher photocatalytic activity (and twelve times higher TOC removal efficiency) than its counterpart prepared by the same method without the application of CS template. Detailed investigation of the optical properties (measured and simulated) of the TiO_2 HS will be the topic of our next report.

Hopefully, our work contributes to the application of renewable, biomass based materials as well as their utilization in effective photocatalytic or energy harvesting processes.

Acknowledgments

The authors wish to express their deepest and sincerest recognition of Prof. András Dombi, a key figure in the topic of photocatalytic materials for the degradation of contaminants of environmental concern. The research and BR were supported by NKFI under the NN 114463 grant and the Swiss Contribution (SH/7/2/20).

Appendix A. Supplementary data

Supplementary data associated with this article can be found, in the online version, at http://dx.doi.org/10.1016/j.cattod.2016.11.038.

References

[1] WHO/UNICEF, Progress on Sanitation and Drinking Water – 2015 Update and MDG Assessment, WHO Press, Geneva, 2015.
[2] WEF, Global Risks 2015, 10th ed., World Economic Forum, Geneva, 2015.
[3] L.H. Keith, W.A. Telliard, Environ. Sci. Technol. 13 (1979) 416–423.
[4] J.T. Yu, E.J. Bouwer, M. Coelhan, Agr. Water. Manage. 86 (2006) 72–80.
[5] J. Michalowicz, W. Duda, Pol. J. Environ. Stud. 16 (2007) 347–362.
[6] S. Ahmed, M.G. Rasul, W.N. Martens, R. Brown, M.A. Hashib, Desalination 261 (2010) 3–18.
[7] S. Ahmed, M.G. Rasul, W.N. Martens, R. Brown, M.A. Hashib, Water Air Soil Pollut. 215 (2011) 3–29.
[8] R. Andreozzi, V. Caprio, A. Insola, R. Marotta, Catal. Today 53 (1999) 51–59.
[9] O. Carp, C.L. Huisman, A. Reller, Prog. Solid State Chem. 32 (2004) 33–177.
[10] A. Fujishima, X.T. Zhang, C. R. Chim. 9 (2006) 750–760.
[11] A. Mills, S. LeHunte, J. Photochem. Photobiol. A 108 (1997) 1–35.
[12] P.V. Kamat, Chem. Rev. 93 (1993) 267–300.
[13] M.A. Henderson, Surf. Sci. Rep. 66 (2011) 185–297.
[14] J.M. Herrmann, Catal. Today 53 (1999) 115–129.
[15] X. Yong, M.A.A. Schoonen, Am. Mineral. 85 (2000) 543–556.
[16] P. Salvador, J. Phys. Chem. C 111 (2007) 17038–17043.
[17] K. Rajeshwar, A. Thomas, C. Janaky, J. Phys. Chem. Lett. 6 (2015) 139–147.
[18] D.C. Hurum, A.G. Agrios, K.A. Gray, T. Rajh, M.C. Thurnauer, J. Phys. Chem. B 107 (2003) 4545–4549.
[19] T. Lopez, R. Gomez, E. Sanchez, F. Tzompantzi, L. Vera, J. Sol-Gel Sci. Technol. 22 (2001) 99–107.
[20] A. Di Paola, M. Bellardita, R. Ceccato, L. Palmisano, F. Parrino, J. Phys. Chem. C 113 (2009) 15166–15174.
[21] G.H. Li, L. Chen, M.E. Graham, K.A. Gray, J. Mol. Catal. A: Chem. 275 (2007) 30–35.
[22] R.G. Nair, S. Paul, S.K. Samdarshi, Sol. Energy Mater. Sol. Cells 95 (2011) 1901–1907.

[23] B. Reti, Z. Major, D. Szarka, T. Boldizsar, E. Horvath, A. Magrez, L. Forro, A. Dombi, K. Hernadi, J. Mol. Catal. A: Chem. 414 (2016) 140–147.
[24] Z. Pap, V. Danciu, Z. Cegled, A. Kukovecz, A. Oszko, A. Dombi, K. Mogyorosi, Appl. Catal. B-Environ. 101 (2011) 461–470.
[25] H.W. Kroto, J.R. Heath, S.C. Obrien, R.F. Curl, R.E. Smalley, Nature 318 (1985) 162–163.
[26] M.M. Titirici, R.J. White, N. Brun, V.L. Budarin, D.S. Su, F. del Monte, J.H. Clark, M.J. MacLachlan, Chem. Soc. Rev. 44 (2015) 250–290.
[27] X.J. He, F.H. Wu, M.D. Zheng, Diam. Relat. Mater. 16 (2007) 311–315.
[28] J.H. Kim, B. Fang, M. Kim, J.S. Yu, Catal. Today 146 (2009) 25–30.
[29] J. Liu, N.P. Wickramaratne, S.Z. Qiao, M. Jaroniec, Nat. Mater. 14 (2015) 763–774.
[30] P. Serp, J.L.s. Figueiredo, Carbon Materials for Catalysis, John Wiley & Sons, Hoboken, N. J, 2009.
[31] A.A. Deshmukh, S.D. Mhlanga, N.J. Coville, Mater. Sci. Eng. R-Rep. 70 (2010) 1–28.
[32] M.M. Titirici, M. Antonietti, N. Baccile, Green Chem. 10 (2008) 1204–1212.
[33] M.M. Titirici, M. Antonietti, Solar Energy Materials and Solar Cells, Chem. Soc. Rev. 39 (2010) 103–116.
[34] M. Iida, T. Sasaki, M. Watanabe, Chem. Mater. 10 (1998) 3780.
[35] R. Rengarajan, P. Jiang, V. Colvin, D. Mittleman, Appl. Phys. Lett. 77 (2000) 3517–3519.
[36] S.H. Hwang, J. Yun, J. Jang, Adv. Funct. Mater. 24 (2014) 7619–7626.
[37] M. Retsch, M. Schmelzeisen, H.J. Butt, E.L. Thomas, Nano Lett. 11 (2011) 1389–1394.
[38] Y. Kondo, H. Yoshikawa, K. Awaga, M. Murayama, T. Mori, K. Sunada, S. Bandow, S. Iijima, Langmuir 24 (2008) 547–550.
[39] M.B. Zheng, J.M. Cao, X. Chang, J. Wang, J.S. Liu, X.J. Ma, Mater. Lett. 60 (2006) 2991–2993.
[40] K.L. Lv, J.G. Yu, K.J. Deng, J. Sun, Y.X. Zhao, D.Y. Du, M. Li, J. Hazard. Mater. 173 (2010) 539–543.
[41] Y. Ao, J. Xu, D. Fu, C. Yuan, Catal. Commun. 9 (2008) 2574–2577.
[42] N. Baccile, G. Laurent, F. Babonneau, F. Fayon, M.M. Titirici, M. Antonietti, J. Phys. Chem. C 113 (2009) 9644–9654.
[43] V. Vashchenko, L. Kutulya, A. Krivoshey, Synthesis-Stuttgart 14 (2007) 2125–2134.
[44] B. Manoj, A.G. Kunjomana, Int. J. Electrochem. Sci. 7 (2012) 3127–3134.
[45] T. Szabo, O. Berkesi, P. Forgo, K. Josepovits, Y. Sanakis, D. Petridis, I. Dekany, Chem. Mater. 18 (2006) 2740–2749.
[46] E. Fuente, J.A. Menendez, M.A. Diez, D. Suarez, M.A. Montes-Moran, J. Phys. Chem. B 107 (2003) 6350–6359.
[47] S.L. Iconaru, F. Ungureanu, A. Costescu, M. Costache, A. Dinischiotu, D. Predoi, J. Nanomater. (2011).
[48] C. Wang, B.L. Dou, Y.C. Song, H.S. Chen, M.J. Yang, Y.J. Xu, Energy Fuel 28 (2014) 3793–3801.
[49] R.A. Spurr, H. Myers, Anal. Chem. 29 (1957) 760–762.
[50] R. Takahashi, S. Sato, T. Sodesawa, M. Kawakita, K. Ogura, J. Phys. Chem. B 104 (2000) 12184–12191.
[51] G. Li, K.A. Gray, Chem. Phys. 339 (2007) 173–187.
[52] D.C. Hurum, K.A. Gray, T. Rajh, M.C. Thurnauer, J. Phys. Chem B 109 (2005) 977–980.
[53] R.I. Bickley, T. Gonzalez-Carreno, J.S. Lees, L. Palmisano, R.J.D. Tilley, J. Solid State Chem. 92 (1991) 178–190.
[54] M. Andersson, L. Osterlund, S. Ljungstrom, A. Palmqvist, J. Phys. Chem. B 106 (2002) 10674–10679.